



HAL
open science

High-Throughput Synthesis and Screening of Functional Coacervates Using Microfluidics

Thomas Beneyton, Celina Love, Mathias Girault, T.-y Dora Tang,
Jean-Christophe Baret

► **To cite this version:**

Thomas Beneyton, Celina Love, Mathias Girault, T.-y Dora Tang, Jean-Christophe Baret. High-Throughput Synthesis and Screening of Functional Coacervates Using Microfluidics. *ChemSystem-sChem*, 2020, 10.1002/syst.202000022 . hal-02870965

HAL Id: hal-02870965

<https://hal.science/hal-02870965v1>

Submitted on 17 Jun 2020

HAL is a multi-disciplinary open access archive for the deposit and dissemination of scientific research documents, whether they are published or not. The documents may come from teaching and research institutions in France or abroad, or from public or private research centers.

L'archive ouverte pluridisciplinaire **HAL**, est destinée au dépôt et à la diffusion de documents scientifiques de niveau recherche, publiés ou non, émanant des établissements d'enseignement et de recherche français ou étrangers, des laboratoires publics ou privés.

High-Throughput Synthesis and Screening of Functional Coacervates Using Microfluidics

Thomas Beneyton^{+, [a]}, Celina Love^{+, [b, d]}, Mathias Girault,^[a] T.-Y. Dora Tang,^{*, [b, d]} and Jean-Christophe Baret^{*, [a, c]}

To understand how membrane-free subcompartmentalization can modulate biochemical reactions by coupled spatial enzyme localization with substrate and product partitioning, we use microfluidic strategies to synthesize, stabilize and characterize micron-sized functional coacervates in water–oil emulsions. Our methodologies have allowed for the first time to quantitatively characterize partition coefficients of a broad range of different molecules with different coacervate chemistries and to measure

reaction rates of individual subcompartments and their surrounding aqueous environment at the single coacervate level. Our results show that sub-compartmentalisation increases the overall rates of reactions. This bottom-up synthetic strategy for the production of synthetic organelles offers a physical model for membrane-free compartmentalization in biology and provides insights into the role of sub-compartmentalisation in regulating out-of-equilibrium behaviours in biological systems.

1. Introduction

Compartmentalization is an essential feature of life, where hierarchical assembly of sub compartments provides a way to spatially organize biology. Cellular micro and nano-compartments allows distinct chemical environments to coexist and support multi-step reactions. In addition, compartmentalization supports the generation and sustenance of chemical gradients essential to maintain out-of-equilibrium processes in cells.^[1] Oparin hypothesized that compartmentalization would have been crucial at the onset of life to enable the organization of chemical and biochemical reactions by providing chemical centers in which selected molecules were concentrated for prebiotic chemistry and/or biology.^[2–9] In modern biology it is well known that compartmentalization occurs across length scales, from the sub-cellular level to the macroscopic assembly of compartments in multicellular organisms. Compartmentaliza-

tion is based on membrane bound compartments such as the mitochondria, nucleus and Golgi apparatus or on membrane-free droplets such as stress granules or P-granules which are collectively known as condensates. The latter are believed to form *via* a liquid-liquid phase separation process of intrinsically disordered proteins (IDPs), RNA and structured proteins^[10,11] and are hypothesized to regulate biological function by regulating the sequestration and therefore the local concentration of molecules. Whilst these condensates have been hypothesized to have potential implications in disease, gene expression regulation^[12] and signaling,^[13,14] how these membrane free droplets may alter out-of-equilibrium behaviours is still not well understood. It can often be difficult to characterize the sequestration of different molecules into biological condensates *in vivo* due to the molecular complexity and *in vitro* due to the difficulty in expressing and purifying condensate forming proteins.

Coacervate microdroplets formed through liquid-liquid phase separation between oppositely charged polyelectrolytes and small molecules offer an alternative synthetic model to biological condensates as studies have shown that the mechanism of biological condensate formation is partly driven by coacervation.^[15,16] In addition, these chemically enriched membrane-free droplets with a highly charged and crowded interior^[17,18] passively upconcentrate molecules and have been shown to support enzymatic reactions where alterations in diffusion length scales or in secondary structure of enzymes affects the rates of reactions^[19–24] thereby modulating biochemical processes. Artificial systems formed by coacervation will therefore be interesting models to test hypothesis on the dynamic properties of membrane-free organelles and offer new routes to generate controlled mimics of those.

Moreover, coacervates represent interesting materials^[25] and are promising tools in bottom-up synthetic biology, where one of its aims is to construct artificial living systems from elementary ingredients and modules.^[26] Despite their advantages for a range of applications the assembly of functional

[a] Dr. T. Beneyton,⁺ Dr. M. Girault, Prof. J.-C. Baret
Univ. Bordeaux, CNRS
CRPP, UMR 5031
115 avenue Albert Schweitzer
33600 Pessac (France)
E-mail: jean-christophe.baret@u-bordeaux.fr

[b] C. Love,⁺ Dr. T.-Y. D. Tang
Max Planck Institute for Molecular Cell Biology and Genetics
Pfotenhauerstrasse 108
01307 Dresden (Germany)
E-mail: tang@mpi-cbg.de

[c] Prof. J.-C. Baret
Institut Universitaire de France 75005 Paris France

[d] C. Love,⁺ Dr. T.-Y. D. Tang
Cluster of Excellence Physics of Life
TU Dresden, 01062 Dresden (Germany)

[*] These authors contributed equally to this work

 Supporting information for this article is available on the WWW under <https://doi.org/10.1002/syst.202000022>

 © 2020 The Authors. Published by Wiley-VCH Verlag GmbH & Co. KGaA. This is an open access article under the terms of the Creative Commons Attribution Non-Commercial License, which permits use, distribution and reproduction in any medium, provided the original work is properly cited and is not used for commercial purposes.

coacervate-based compartments is hindered by the intrinsic transient nature of the structures and the difficulty in handling and characterizing known concentrations of molecules within the coacervates at the micron scale. Recently, the control of coacervate formation was achieved in micron-sized compartments using microfluidics,^[27,28] with the demonstration that the coacervation process can be controlled by a chemical reaction acting on the molecule that makes up the coacervate. Whilst such a synthetic biology approach represents progress in building structural representations of compartmentalization there still remains key challenges for the synthesis and characterisation of functional model systems that can be produced reliably and robustly in a high throughput manner.

New microfluidic methods for the high-throughput production, functionalisation and analysis of coacervates would provide unprecedented quantitative approaches of molecular dynamic processes on the single droplets level at high throughput and provide rational models for enzymatically active subcompartments as found in biological systems.^[29,30]

To address these issues, we have designed and synthesised an active membrane-free subcompartment with coupled features of localized enzyme reactions and passive molecular sequestration. Structurally, this comprises a coacervate microdroplet surrounded by a finite volume of aqueous media provided by a surfactant stabilized water-in oil droplet. This system allows the flux of reagents and products into and out of the membrane-free compartment, based on the partition coefficient of different solutes and substrates whilst spatially localizing an enzyme reaction (E). (Figure 1a). The surrounding aqueous media acts as a source of substrate (N) and a sink for the waste product (P) produced within the coacervate droplet. Here, we have activated the compartments with an enzyme, formate dehydrogenase, which uses NAD^+ as a co-factor and formate as a substrate producing fluorescent NADH and CO_2 as products (Figure 1b). We use microfluidics to spontaneously form populations of micron-sized membrane-free coacervates from polyelectrolyte mixtures. The use of microfluidics allowed us to build highly stable and robust synthetic cellular systems, to manipulate them and to measure the enzymatic activity accurately and at high-throughput, shedding light on the

underlying mechanism of the transport process. We provide quantitative measurements with statistics over large populations of coacervates. Our quantitative approach demonstrates for the first time that transport in coacervates at the micron scale is driven by equilibrium processes, without energy barriers to partitioning.

2. Results and Discussion

To achieve stable individuated coacervate microdroplets we used microfluidics to spontaneously assemble coacervates within water-in-oil (w/o) droplets. Traditionally, coacervate microdroplets are formed by mixing stock aqueous solutions, by hand, containing either a polycation (Polylysine (Plys) or poly (diallyldimethylammonium chloride) (PDDA)) with a polyanion (carboxymethyl–dextran (CM–Dex) or adenosine triphosphate (ATP)) at fixed molar ratios (Figure S1). When prepared by hand, coacervates were highly polydisperse as observed by optical microscopy (Figure S2), where diameters typically span one order of magnitude (and therefore volumes vary over three orders of magnitude). We observe that the droplets coarsen with a continuous change of coacervate size distribution over timescales ranging from hours to days. Eventually, all of the droplets coalesce to form a single coacervate phase in equilibrium with the continuous phase.

A flow-focusing microfluidic device was used to co-encapsulate the coacervate components in 30 pL w/o droplets stabilized by 3% (w/w) of perfluoropolyether–polyethyleneglycol block-copolymer surfactant (PPE–PEG–PFPE) (Figure 2a, Figure S3). Typically, the final monomer molar ratio of the polycation and polyanion are fixed at the beginning of the experiment, prior to flow focusing, at 4:1 molar ratio $\text{Plys}:\text{ATP}$ and $\text{PDDA}:\text{ATP}$ and 6:1 for $\text{CM–Dex}:\text{PDDA}$ and $\text{CM–Dex}:\text{Plys}$. Coacervate formation occurs within the w/o droplets as an additional stream of water is co-flowed between the two streams of polyelectrolytes to prevent mixing of the polycation and polyanion prior to encapsulation. After encapsulation and mixing, the formation of sub-micron sized droplets occurs and these droplets coarsen over time *via* coalescence to form a single coacervate droplet within each w/o droplet (Figure 2a). For a given composition, we obtain w/o droplets and coacervates of identical sizes, with a high level of monodispersity and low levels of size variability on the order of 2–4% which is close to the noise of the image processing algorithm used (Figure S4). The high monodispersity of the w/o droplets is reflected in the monodispersity of the intracellular coacervate organelles and is the direct consequence of efficient and equivolume encapsulation of the coacervate components within the w/o droplets and of the ability for the system to quickly reach an equilibrium state in each droplet. No wetting of the droplet interface by the coacervate is observed indicating negligible interactions between the polyelectrolytes and the surfactant. Our results demonstrate that the assembly process is robust and reproducible (Figure 2b, c, Figure S4). The final size of the coacervate droplets is further controlled by varying the initial concentrations of the coacervate components at fixed

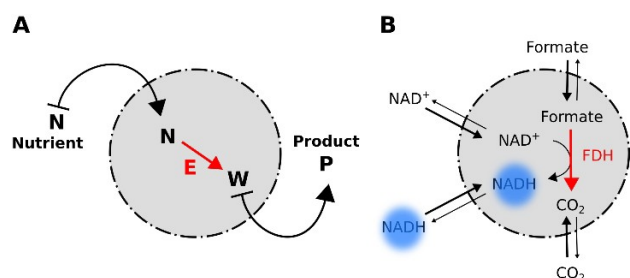


Figure 1. Principle of activated membrane-free organelles. (A) Coacervates interact with their surrounding environment to (i) uptake nutrient N; (ii) process it by the activity of a sequestered enzyme E and (iii) release the product P. (B) Model of functional coacervate. Formate dehydrogenase (FDH) is sequestered in the coacervate. Formate substrate and NAD^+ (cofactor) are uptaken and processed by FDH in the microcompartment. NADH and carbon dioxide (CO_2) are then released.

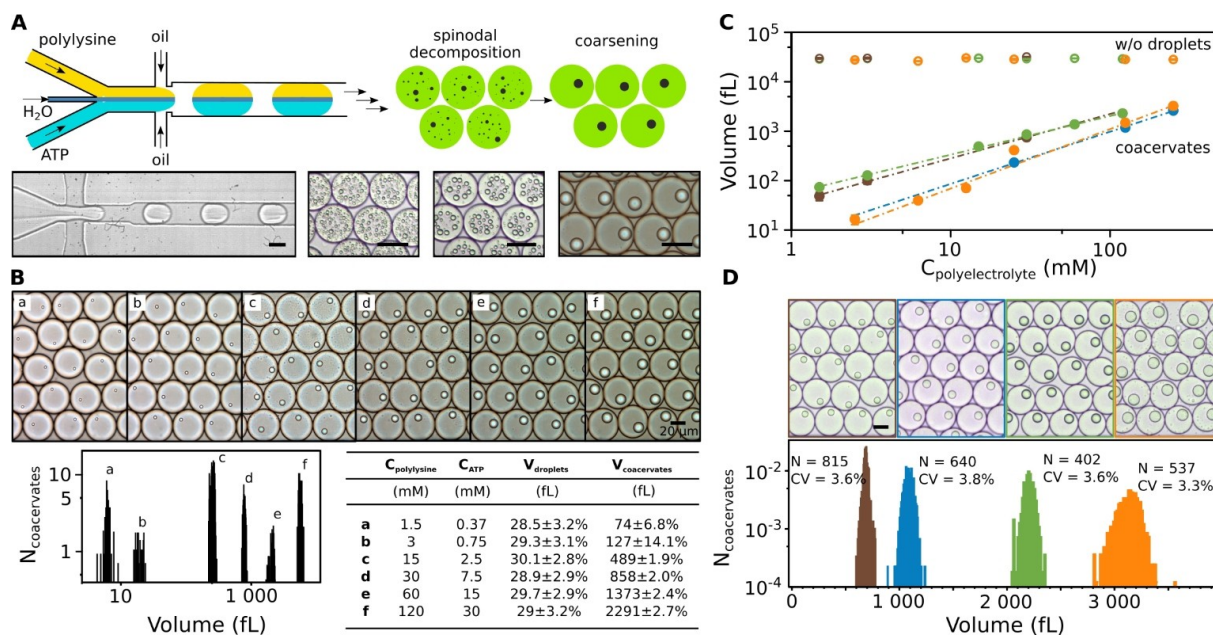


Figure 2. Microfluidic control of coacervation. (A) Coacervate formation. Co-encapsulation of oppositely charged polylysine and ATP induces liquid-liquid phase separation by coacervation within w/o droplets and leads to single coacervate droplet in each water/oil droplet. Bright-field images of the templated coacervation process. Scalebar 30 μm . (B–C) Size control. (B) Bright-field images of 30 pL droplets with increasing initial concentrations of Polylysine/ATP system. The volume of the coacervates is estimated using an image analysis routine. (C) Dependency of the coacervate volume with respect to the initial w/o droplet composition for the Plys/ATP (green), PDDA/ATP (brown), CM-Dex/Polylysine (orange) and CM-Dex/PDDA (blue) systems. Respective w/o droplet volumes are shown (open circles). (D) Coacervate stability. Bright-field images of 30 pL droplets after incubation at 25 °C for 107, 112, 107 and 81 days in the case of the PDDA/ATP (brown), CM-Dex/PDDA (blue), Plys/ATP (green) and CM-Dex/Plys (orange) systems respectively. The volume of the coacervates is estimated using an image analysis routine. Scale bar 30 μm .

molar ratio (Figure 2b, Figure S5). The coacervate droplet size is varied over two orders of magnitude in volume, from 30 fL to 3 pL (Figure 2c). We obtain a power law scaling with a non-universal exponent which varies depending on the coacervate system where the CM-Dex based coacervates have an exponent of between 1.04 and 1.18 and the ATP based coacervates display an exponent between 0.79 and 0.9. Deviations from a linear relationship between concentration and size of the coacervates may be attributed to additional electrostatic effects from salt ions, for example, as a function of increasing polyelectrolyte concentration.^[31] Interestingly, we also observe that the concentration of the coacervate components affect the kinetics of the coacervate macrophase equilibration. While the initial formation of the coacervate “seeds” within the water–oil emulsion is fast (less than 1 s), the time scale for coarsening is tuned from seconds to days by changing the initial concentrations from 100 to 1 mM. Reducing the initial concentration leads to an increase in the coarsening timescale, with systems prepared at low initial concentrations remaining in an uncoalesced metastable state for months. This result implies that the nucleation process is not the rate limiting step in the phase separation process, as observed recently.^[28] Equilibrium is mainly limited by the coarsening process, even at small dimensions where diffusion is fast. All further experiments were performed with concentrations of polyelectrolytes for which coarsening of the coacervate droplets into a single droplet/organelle occurs within seconds.

Once formed, the coacervates are stable in the droplets after three months of incubation, at room temperature, with no observed impact on their size or structural integrity (Figure 2d). The stability of the coacervate population is dependent on the stability of the w/o emulsion, which is typically one year with the formulation used.^[32,33] We observe similar features of nucleation growth to produce single monodisperse coacervate droplets compared to those produced in lipid vesicles.^[27,34] (NOTE OF THE AUTHORS: We would like to add here after ref 34 the reference: C. Love, J. Steinkühler, D. T. Gonzales, N. Yandrapalli, T. Robinson, R. Dimova, T.-Y. D. Tang, *Angew. Chem. Int. Ed.* **2020**, *59*, 5950) Our results confirm that microfluidics is efficient in producing high numbers of highly stable monodisperse coacervates with specific chemical compositions within w/o droplets.

Typically, solutes or chaperone molecules partition into the coacervate phase depending on their chemical properties.^[18,35–38] At thermodynamic equilibrium, the concentration distribution of the solutes within the coacervate droplet and outside of the coacervate droplet is determined by the chemical potential of the added molecules in each phase and reduces for dilute solutions to a single parameter, the partition coefficient (K). The partitioning is driven by the difference in interactions of the solutes with the coacervate matrix. As the partition coefficient depends on a number of factors including the intrinsic chemical, structural, and dielectric differences between the molecularly crowded coacervate matrix and the surrounding environment,^[39,40] it is important to characterize

the partitioning of a range of different molecules. In addition, because the transport of molecules across the coacervate interface regulates the reaction dynamics of membrane-free compartmentalization, a further understanding of whether molecular transport across the coacervate interface is kinetic-limited or diffusion-limited is required. In bulk, measuring the partition coefficient of a chaperone molecule can often be lengthy and costly using large volumes of sample.

We, therefore, used a high-throughput microfluidic approach to measure the partition coefficient at the single coacervate level. Our method is derived from the analysis of single cells in microfluidics^[41] using a fluorescence signal as a reporter of the concentrations of the solutes in each of the phases (Figure 3a–d, Figure S6). Both the fluorescence inside (F_c) and outside (F_d) the coacervates are measured and the partition coefficient, K , is obtained from the ratio F_c over F_d . In a typical experiment, a four-bit emulsion,^[42] *i.e.* containing four populations of different compositions, is produced in order to expose coacervate droplets to four concentrations of a given

molecule (Supporting Information). As shown in Figure 3e, the F_c/F_d ratio is independent from the fluorescein concentration for our experiments. These results confirm that the chemical potentials equilibrate inside and outside of the coacervates to reach thermodynamic equilibrium. Using this platform, we measured the partition coefficient of different solutes to untangle general trends in partitioning within different coacervate systems (Figure 3f, Figure S7).

We have characterized the molecules that are required for the formate dehydrogenase reaction and have extended our study to other biological molecules. Specifically, the solutes include fluorescein (0.3 kDa, neutral), NADH (0.7 kDa, negatively charged) and biological macromolecules in the form of proteins; FITC-labelled β -galactosidase (46 kDa), FITC-labelled formate dehydrogenase (74 kDa) and nucleotides such as a FITC-labelled double-stranded DNA (15 kDa). As a general trend, small organic molecules tend to be more labile and partition less than larger biomolecules such as proteins or oligonucleotides. Double-stranded DNA partitioned efficiently in both positively-

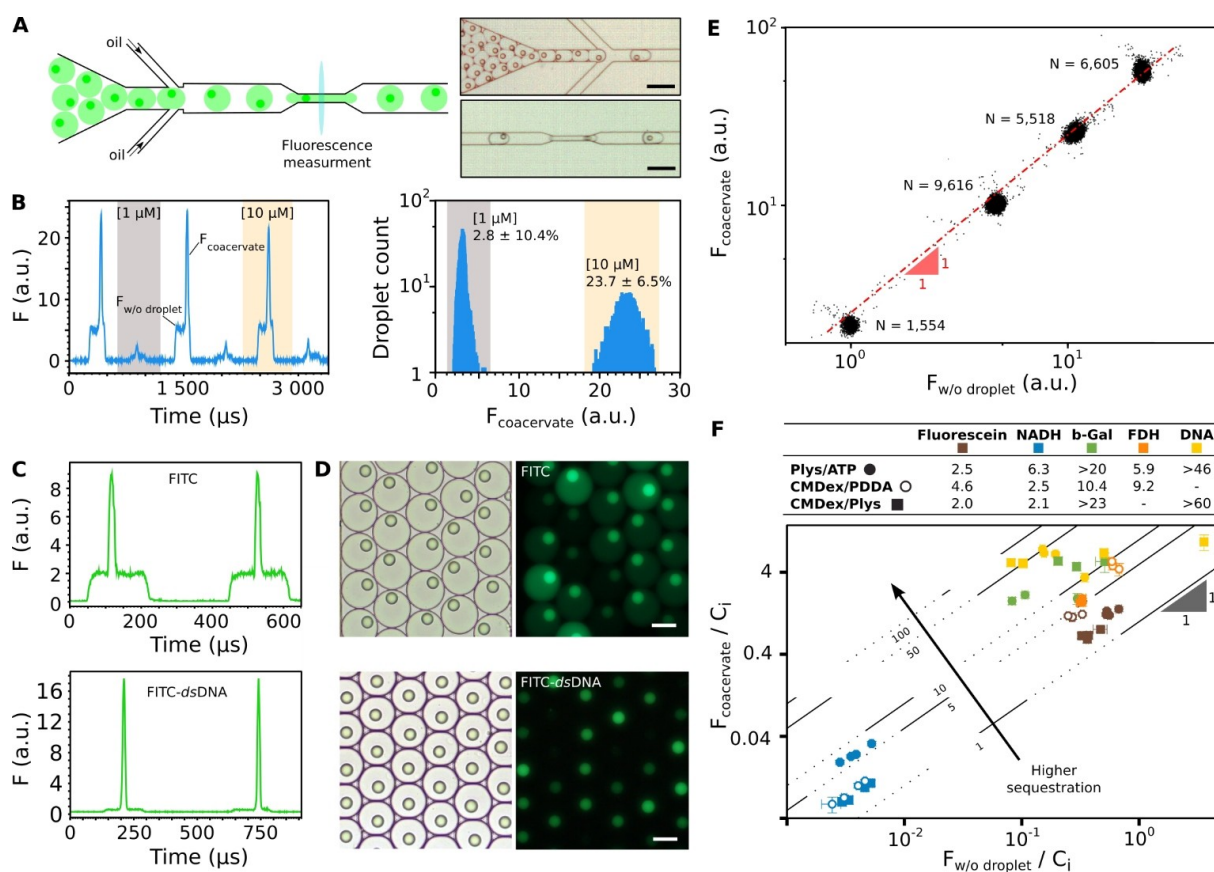


Figure 3. Selective sequestration of molecules. (A–B) Fluorescence measurement. (A) Sketch of the fluorescence detection device. (B) Time sequence of the fluorescence signal of a binary emulsion in the case of CM–Dex/PDDA (168 mM/28 mM) with either 1 or 10 μ M of Dextran-cascade blue coding dye. The fluorescence inside (F_c) and outside (F_d) coacervates are monitored. Distribution of F_c at the population level in the case of the same binary emulsion. $N = 40\,000$. (C–F) Sequestration efficiency. (C) Time sequence of the fluorescence signal in the case of Plys/ATP (100 mM/25 mM) with 84 μ M fluorescein (Top) or 4.3 mM FITC-labelled double-stranded DNA (Bottom). (D) Bright-field and fluorescence pictures of 4-bit emulsions containing Plys/ATP (100 mM/25 mM) and fluorescein (either 3, 17, 42 or 84 μ M – Top) or FITC-dsDNA (either 0.7, 2, 3.3 or 4.3 mM – Bottom). Scalebar 30 μ m. (E) Example of F_d vs. F_c 2D plot in the case of Plys/ATP (100 mM/25 mM) for a 4-bit emulsion with either 3, 17, 42, 84 μ M fluorescein. (F) Partitioning coefficients obtained from F_d vs. F_c plots for Fluorescein (brown), NADH (blue), FITC-tagged beta-galactosidase (green), FITC-tagged formate dehydrogenase (orange) and DNA (yellow) in the case of the Plys/ATP (circles), CM–Dex/PDDA (open circles) and CM–Dex/Plys (squares) systems. The table summarizes the corresponding measured partition coefficients. The values reported as lower bound values are limited by the signal to noise ratio at low concentrations (Supporting information).

charged ($K \sim 43$) and negatively-charged ($K \sim 58$) coacervates. Similar to DNA, proteins partitioned efficiently in coacervates, even though β -galactosidase showed higher partition coefficients than FDH ($K \sim 10$ – 20 and ~ 5 – 10 respectively) while NADH or fluorescein have a partition coefficient in the order of 2–6 depending on the coacervate matrix. For example, NADH, which has two negative charges at pH=8, partitioned more efficiently into positively-charged Plys/ATP ($K \sim 6.4$) coacervates rather than in negatively-charged CM–Dex/PDDA ($K \sim 2.5$) or CM–Dex/Plys ($K \sim 2.1$) coacervates. The results indicate that partitioning of smaller molecules such as NADH is driven by electrostatic interactions between NADH and the overall positively charged coacervate system (Plys/ATP). In addition, fluorescein ($pK_a = 6.4$) partitions two to three times more strongly into the CM–Dex/PDDA compared to CM–Dex/Plys. This observation may be attributed to the difference in charge interaction of fluorescein between the primary amine on polylysine and the tertiary ammonium cation on PDDA. For negatively charged molecules, the higher partitioning of larger molecules (DNA) into coacervates with a greater negative charge ratio is likely a combination of entropic effects (related to the configurations of the macromolecules in the coacervate compared to smaller molecules such as NADH) and of a higher binding constant of DNA to the positively charged component than the coacervate anion. It is important to note, that we do not consider variations in quantum efficiency of the fluorophores in the coacervate phase and its surrounding aqueous phase. This may be important when local concentrations reach the limit of self-quenching. However, in these experiments the concentrations of solutes are below this limit. In addition, changes to the partition coefficients due to the addition of the barcoding dye cannot be entirely ruled out. Here, these errors are negligible as the linearity observed in Figure 3e suggests that fluorescence is not quenched at high concentrations.

Our experiments offer new routes to quantify molecular sequestration in single membrane-free coacervate droplets at high-throughput. The method can be generalized to a variety of experimental systems, provided that proper calibration of the fluorescence as a function of concentration is performed in each of the phases. We demonstrate that sequestration is in thermodynamic equilibrium where the molecules are freely diffusing into and out of the droplet. The large value of the partition coefficient for DNA and proteins shows the spontaneous sequestration of information carrying biological macromolecules and demonstrate the ability for coacervate organelles to passively link phenotype and genotype by incorporation of both nucleic acid polymers (genotype) and polypeptides (phenotype).

In order to generate an enzymatically activated organelle, we include the formate dehydrogenase reaction into the synthetic organelle as described in Figure 1b. The reaction was monitored by measuring the intrinsic fluorescence of NADH^[42] to probe the effect of enzymatic reactions in single coacervate droplets in contact with a finite volume of aqueous phase (defined here as a coupled system) and compared to bulk phase measurements, where coacervate and aqueous phases are not in contact at equivalent concentrations (defined here as the

uncoupled system). We first tested the viability of the coacervate microenvironment for supporting enzymatic reactions. By using the bulk coacervate phase only, we avoid any effects from diffusion of the product into the coacervate phase that may be generated from spurious enzyme reactions taking place in the external aqueous phase. Formate dehydrogenase (0.1 U.ml^{-1}), sodium formate (25 mM) and the co-factor NAD⁺ (600 μM) are incorporated into either CM–Dex:PDDA (6:1 molar ratio) and Plys:ATP (4:1 molar ratio) bulk coacervate phase and the kinetics of the reaction are obtained from monitoring NADH formation by fluorescence spectroscopy (see materials and methods). Sodium formate is in excess stoichiometric conditions. The initial rates of reaction are obtained by fitting the kinetic curves to a single exponential and obtaining the first differential at $t = 0$ sec. Our results show that formate dehydrogenase is active within both coacervate systems, with an increase in the initial rate observed in both of the CM–Dex/PDDA and Plys/ATP coacervate phases compared to the buffer solution (Figure 4a,b).

The enzymatic reaction was then loaded into our coacervate-based organelle by co-flowing formate dehydrogenase (FDH) and NAD⁺ with the coacervate components to generate a w/o emulsion. As previously described, a four-bit emulsion was produced with four different populations of coacervates barcoded with sulforhodamine B. The four populations are respectively composed of (i) coacervate and FDH, (ii) coacervate without FDH (negative control), (iii) FDH without coacervation (bulk reaction) and (iv) coacervate with, FDH and NADH (internal reference of fluorescence). The four-bit emulsions were analyzed in a kinetic device (Figure 4c, Figure S8). The enzymatic substrate was then picoinjected^[43] into w/o droplets which were incubated on-chip in delay lines. The fluorescence intensities (F_c and F_d) of NADH were measured at different incubation time using laser focusing as described in Figure 2a. The kinetics of NADH production over time was measured at a cellular population size of approximately 1,000 coacervates for both CM–Dex/PDDA and Plys/ATP systems (Figure 4d, Figure S9). Initial rates of the reaction were obtained as previously described and compared to the initial rates of NADH production for bulk coacervate phase and supernatant solutions only. In order to directly compare the initial rates of reaction within the coupled system (hybrid artificial cell) and uncoupled system (bulk coacervate phase or bulk supernatant phase only), the partition coefficients obtained using microfluidic techniques were used to calculate the expected concentration of formate dehydrogenase and NAD⁺ within the coacervate organelle and aqueous phase in the w/o emulsions. Sodium formate (18.5 mM or 26.5 mM) was always added in excess and therefore variation in its concentration was assumed not to affect the initial rates of reaction. From our partition coefficient experiments we calculated an increase in formate dehydrogenase concentration to 0.45 U.ml^{-1} in the coacervate microdroplet and a decrease in the enzyme concentration to 0.05 U.ml^{-1} within the aqueous phase. The greater concentration of the enzyme and cofactor in the coacervate droplet compared to the aqueous phase leads to the observed increase in initial rate of reaction (Figure 4d,e). As our bulk partition coefficients, based on absorbance

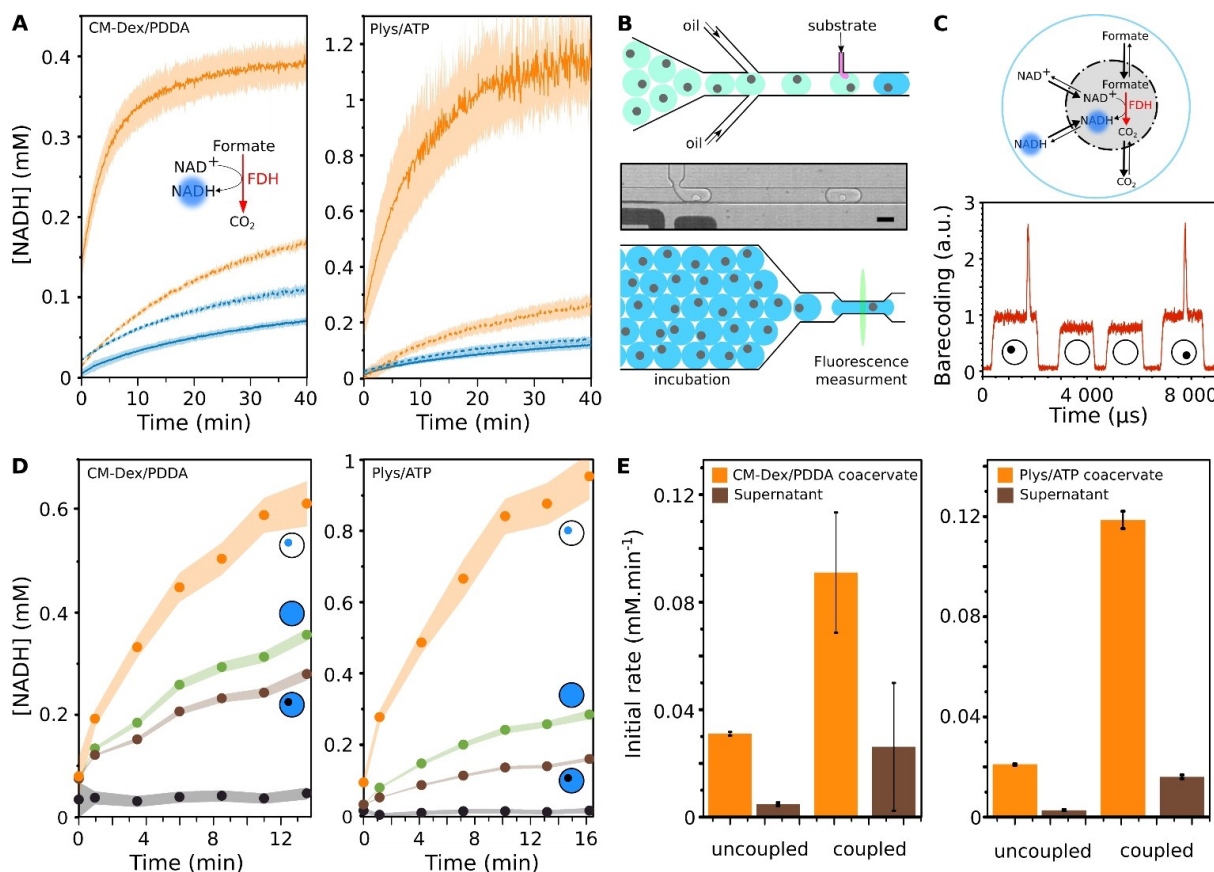


Figure 4. Spatial organization of enzymatic reactions in coacervate-based organelles. (A) Formate dehydrogenase activity in bulk macrophases for CM–Dex/PDDA (168 mM/28 mM) (left) and Plys/ATP (100 mM/25 mM) (right). NADH concentration versus time in the coacervate phase (orange) and the depleted phase (blue) after partitioning sodium formate, macrophases separation and addition of FDH and NADH at equal concentrations (dashed lines) or with a concentration ratio based on its partition coefficient (plain lines). (B) Sketch of the kinetics device. The metabolic substrate is picoinjected, droplets are incubated on-chip and fluorescence in both coacervate and depleted phases are measured at different incubation time points. (C) Sketch of the sequestered formate dehydrogenase reaction: w/o droplet with a coacervate-based organelle functionalized with FDH. Time sequence of the fluorescence signal (barcoding, sulforhodamine B) of a binary emulsion composed of w/o droplets with or without coacervation (containing only one coacervation component with similar total molarity). (D) NADH concentration versus time inside coacervates (orange), outside coacervates (brown) or in w/o droplets without coacervation (green) in the case of CM–Dex/PDDA (168 mM/28 mM) (left) or Plys/ATP (100 mM/25 mM) (right) systems. A negative control in black shows coacervates without FDH. (E) Initial rates of FDH reaction in the coacervate and in the depleted phase for the uncoupled (bulk) or coupled (w/o droplets) situations in the case of CM–Dex/PDDA (168 mM/28 mM) (left) or Plys/ATP (100 mM/25 mM) (right).

spectroscopy, show that NAD^+ and NADH have the same partition coefficient within error (Table S1), we expect a concentration of 0.90 mM of NAD^+ within the coacervate microdroplet and 0.36 mM in the aqueous phase. At these concentrations, the initial rates of the formate dehydrogenase reaction are compared between the coupled and uncoupled system (Figure 4e). Our results show that the initial rate is greater in both the coacervate microdroplet and the aqueous phase within the coupled system compared to the uncoupled system. The increased rate in the aqueous phase coupled to the coacervate droplet is a direct consequence of both the high rate of production inside the coacervate and the almost instantaneous partitioning of NADH into the coacervate's surrounding aqueous phase to equilibrate the chemical potential of the product between both phases. Due to the requirement to maintain the partition coefficient, the coacervate external phase acts as a sink partitioning NADH from the coacervate organelle into the aqueous surrounding leading to a

higher apparent initial rate in the surrounding aqueous phase compared to the uncoupled system (aqueous phase alone).

There are several possibilities to explain the increase in the rate of reaction within the coacervate microdroplet within the w/o emulsion. One possibility is that the NAD^+ concentration is incorrectly estimated. We measured the partition coefficients of NAD^+ and NADH using bulk methodologies and UV absorbance and obtained $K_{\text{NAD}^+} = 2.22 \pm 0.23$ and $K_{\text{NADH}} = 3.13 \pm 0.39$ respectively showing that there is an overestimation of approximately 40% in NAD^+ concentration partitioned into the coacervate phase based on NADH fluorescence. Control experiments with approximately 60% increase in the NAD^+ concentration shows an increase in the rate of reaction (Figure S10) which is less than the observed increase in the coupled systems (Figure 4e). The increase in the initial rate within the coacervate droplet could be attributed to a shift in the equilibrium of the reaction related to the removal of the product from the coacervate droplet into the surrounding aqueous phase. In

addition, this effect could in principle even strengthen other types of chemical reaction. For example, where the product inhibits the active site of an enzyme, as is the case for the formate dehydrogenase reaction,^[44,45] the reaction would be maintained and the rates increased in the droplet, provided that the transport of the product into the external phase is effective. In contrast, our system would decrease the efficiency of autocatalytic reactions as product would be removed from the reaction centre, *i.e.* the coacervate droplet. The Plys/ATP coacervates show the same general trends as those observed for CM–Dex/PDDA with increases in initial rates observed in both the coacervate droplet and its surrounding aqueous phase in the coupled system compared to the uncoupled system (Figure 4e). The analysis of the partition coefficients as a function of time shows that the Plys/ATP system reaches a steady state after 4 mins compared to 9 mins for CM–Dex/PDDA system (Figure S11). This shows that altering the chemistries of the coacervate droplet may affect the kinetics but the general trends remain consistent between systems. As a final note, we want to highlight the interest of our system to obtain quantitative information on the kinetics of enzymes in small compartments. Although this was not the focus of our work here, our systems can be adapted to quantitatively determine the kinetic parameters of enzymes, but requires modeling of the equilibrium between phases for a reliable quantification of the parameters.

3. Conclusion

Liquid droplets formed via coacervation are interesting synthetic models of biological condensates because they display a number of important structural and functional properties that mimic *in vivo* membrane-free droplets. Here, we show that microfluidic formation of synthetic microdroplets formed by liquid-liquid phase separation processes, such as coacervation, integrated with water–oil emulsions provide a universal platform as subcompartmentalised biosynthetic reaction centers. We show that a functional synthetic organelle coupled to an external aqueous environment recruits reactant molecules from the external aqueous phase via passive sequestration, executes the reaction in the coacervate and releases the product in the external phase via sequestration to maintain the partition coefficient of the system. By monitoring the rate of reaction, we show an increase in the rate of product formation within the coacervate organelle compared to the bulk phase measurements, where coacervate and aqueous phases are uncoupled at equivalent concentrations.

Whilst we have focused on the formate dehydrogenase reaction as part of the model system, our approach constitutes a universal route to study and control systems which undergo liquid-liquid phase separation and provides a new framework to understand, control and use elementary physico-chemical phenomena associated to membrane-free compartmentalization. The ability to induce a flux of chemicals driven by the activity within the coacervate has important consequences for building out-of-equilibrium systems. A recent theoretical study

predicts that droplets which support chemical reactions whilst allowing the bidirectional flux of molecules across the droplet interface will lead to droplet division.^[46] These approaches therefore suggest that elementary biological functions such as chemical energy harvesting from the environment and cellular division can be integrated in minimal systems based on coacervates. Coacervate-based systems can now be engineered and functionalized in a bottom-up approach, therefore taking a step towards the creation of functional artificial cells. In the future, these cells may transition from an inanimate to a living state, provided that a sufficient number of functionalities are integrated in the compartments.

Experimental Section

All experimental details are provided in the Supporting Information.

Acknowledgements

All authors acknowledge funding from the Max Syn Bio consortium, jointly funded by the Federal Ministry of Education and Research of Germany and the Max Planck Society. J.-C.B. acknowledges financial support by the ERC (FP7/2007-2013/ERC Starting Grant Sofi), from the French state in the frame of the 'investment for the future', Programme IdEx Bordeaux, ANR-10-IDEX-03-02, from the Région Nouvelle Aquitaine. MG. acknowledges financial support by the European Program H2020 (MSCA-797007). TYDT acknowledges the Cluster of Excellence, Physics of Life, TU Dresden and EXC-1056 for funding and Tony Hyman for useful discussions.

Conflict of Interest

The authors declare no conflict of interest.

Keywords: coacervates · microfluidics · out-of-equilibrium · soft matter · synthetic chemistry

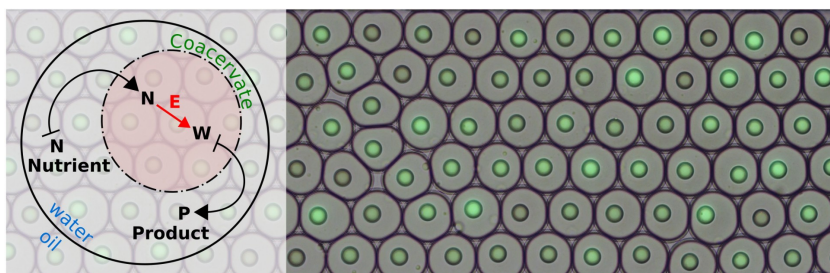
- [1] S. F. Banani, H. O. Lee, A. A. Hyman, M. K. Rosen, *Nat. Rev. Mol. Cell Biol.* **2017**, *18*, 285–298.
- [2] A. Cairns-Smith, *Genetic Takeover and the Mineral Origins of Life*, Cambridge University Press, New York, **1982**.
- [3] C. Thaxton, W. Bradley, R. Olsen, *The Mystery of Life's Origin*, Philosophical Library Inc., New York, **1984**.
- [4] C. R. Woese, *J. Mol. Evol.* **1979**, *13*, 95–101.
- [5] C. Darwin, *The Life and Letters of Charles Darwin: Including an Autobiographical Chapter*, Cambridge University Press, **2009**.
- [6] J. B. S. Haldane, *Ration. Annu.* **1929**, *148*, 3–10.
- [7] A. I. Oparin, *Proiskhozhdenie Zhizny*, Izd. Mosk. Rabochii, Moscow, **1924**.
- [8] C. de Duve, *Blueprint for a Cell: The Nature and Origin of Life*, Neil Paterson Publisher, Burlington, North Carolina, **2003**.
- [9] S. Mann, *Angew. Chem. Int. Ed.* **2013**, *52*, 155–162; *Angew. Chem.* **2013**, *125*, 166–173.
- [10] A. A. Hyman, C. A. Weber, F. Jülicher, *Annu. Rev. Cell Dev. Biol.* **2014**, *30*, 39–58.
- [11] A. A. Hyman, K. Simons, *Science* **2012**, *337*, 1047–1049.

- [12] S. F. Banani, H. O. Lee, A. A. Hyman, M. K. Rosen, *Nat. Rev. Mol. Cell Biol.* **2017**, *18*, 285–298.
- [13] W. Y. C. Huang, S. Alvarez, Y. Kondo, Y. Kwang Lee, J. K. Chung, H. Y. Monatrice Lam, K. H. Biswas, J. Kuriyan, J. T. Groves, *Science* **2019**, *363*, 1098–1103.
- [14] L. B. Case, X. Zhang, J. A. Ditlev, M. K. Rosen, *Science* **2019**, *363*, 1093–1097.
- [15] C. W. Pak, M. Kosno, A. S. Holehouse, S. B. Padrick, A. Mittal, R. Ali, A. A. Yunus, D. R. Liu, R. V. Pappu, M. K. Rosen, *Mol. Cell* **2016**, *63*, 72–85.
- [16] C. P. Brangwynne, C. R. Eckmann, D. S. Courson, A. Rybarska, C. Hoeghe, J. Gharakhani, F. Jülicher, A. A. Hyman, *Science* **2009**, *324*, 1729–1732.
- [17] J. T. G. Overbeek, M. J. Voorn, *J. Cell. Physiol. Suppl.* **1957**, *49*, 7–22.
- [18] P. Zhang, N. M. Alsaifi, J. Wu, Z.-G. Wang, *J. Chem. Phys.* **2018**, *149*, 163303.
- [19] B. Elowitz, M. G. Surette, M. P.-E. Wolf, B. Stock, J. S. Leibler, *J. Bacteriol.* **1999**, *181*, 197–203.
- [20] B. Drobot, M. Iglesias-Artola, J. K. Le Vay, V. Mayr, M. Kar, M. Kreysing, H. Mutschler, T.-Y. Dora Tang, *Nat. Commun.* **2018**, *9*, 3643.
- [21] A. Dhar, A. Samiotakis, S. Ebbinghaus, L. Nienhaus, D. Homouz, M. Gruebele, M. S. Cheung, *Proc. Natl. Acad. Sci. USA* **2010**, *107*, 17586–17591.
- [22] T. Pereira de Souza, F. Steiniger, P. Stano, A. Fahr, P. Luisi, *ChemBioChem* **2011**, *12*, 2523–2530.
- [23] E. Sokolova, E. Spruijt, M. M. K. Hansen, E. Dubuc, J. Groen, V. Chokkalingam, A. Piruska, H. A. Heus, W. T. S. Huck, *Proc. Natl. Acad. Sci.* **2013**, *110*, 11692–11697.
- [24] T.-Y. Dora Tang, D. van Swaay, A. deMello, J. L. Ross Anderson, S. Mann, *Chem. Commun.* **2015**, *51*, 11429–11432.
- [25] J. M. Horn, R. A. Kapelner, A. C. Obermeyer, *Polymers (Basel)*. **2019**, *11*, 578.
- [26] P. Schwillie, J. Spatz, K. Landfester, E. Bodenschatz, S. Herminghaus, V. Sourjik, T. Erb, P. Bastiaens, R. Lipowsky, A. Hyman, P. Dabrock, J.-C. Baret, T. Vidakovic-Koch, P. Bieling, R. Dimova, H. Mutschler, T. Robinson, T.-Y. D. Tang, S. Wegner, K. Sundmacher, *Angew. Chem. Int. Ed.* **2018**, DOI 10.1002/anie.201802288.
- [27] V. Deshpande, F. Brandenburg, A. Lau, M. G. F. Last, W. Kasper Spoelstra, L. Reese, S. Wunna, M. Dogterom, C. Dekker, *Nat. Commun.* **2019**, *10*, 1800.
- [28] M. Linsenmeyer, M. R. G. Kopp, F. Grigolato, D. Liu, D. Zürcher, M. Hondele, K. Weis, U. Capasso Palmiero, P. Arosio, *Angew. Chem. Int. Ed.* **2019**, *58*, 1–7.
- [29] A. I. Oparin, *Adv. Enzymol. Relat. Areas Mol. Biol.* **1965**, *27*, 347–380.
- [30] D. Zwicker, R. Seyboldt, C. A. Weber, A. A. Hyman, F. Jülicher, *Nat. Phys.* **2017**, *13*, 408–413.
- [31] L. Li, S. Srivastava, M. Andreev, A. B. Marciel, J. J. de Pablo, M. V. Tirrell, *Macromolecules* **2018**, *51*, 2988–2995.
- [32] J.-C. Baret, *Lab Chip* **2012**, *12*, 422–433.
- [33] P. Gruner, B. Riechers, L. A. Chacón Orellana, Q. Brosseau, F. Maes, T. Beneyton, D. Pekin, J. C. Baret, *Curr. Opin. Colloid Interface Sci.* **2015**, *20*, 183–191.
- [34] N. N. Deng, W. T. S. Huck, *Angew. Chem. Int. Ed.* **2017**, *56*, 9736–9740; *Angew. Chem.* **2017**, *129*, 9868–9872.
- [35] K. A. Black, D. Priftis, S. L. Perry, J. Yip, W. Y. Byun, M. Tirrell, *ACS Macro Lett.* **2014**, *3*, 1088–1091.
- [36] S. Koga, D. S. Williams, A. W. Perriman, S. Mann, *Nat. Chem.* **2011**, *3*, 720–724.
- [37] D. S. Williams, S. Koga, C. R. C. Hak, A. Majrekar, J. Patil Avinash, A. W. Perriman, S. Mann, *Soft Matter* **2012**, *8*, 6004–6014.
- [38] T.-Y. D. Tang, M. Antognozzi, J. A. Vicary, A. W. Perriman, S. Mann, *Soft Matter* **2013**, *9*, 7647–7656.
- [39] M. Li, X. Huang, T.-Y. D. Tang, S. Mann, *Curr. Opin. Chem. Biol.* **2014**, *22*, 1–11.
- [40] W. M. Aumiller Jr, C. D. Keating, *Nat. Chem.* **2016**, *8*, 129–137.
- [41] H. Lu, O. Caen, J. Vrignon, E. Zonta, Z. El Harrak, P. Nizard, J. C. Baret, V. Taly, *Sci. Rep.* **2017**, *7*, DOI 10.1038/s41598-017-01454-4.
- [42] T. Beneyton, D. Krafft, C. Bednarz, C. Kleineberg, C. Woelfer, I. Ivanov, T. Vidaković-Koch, K. Sundmacher, J.-C. Baret, *Nat. Commun.* **2018**, *9*, 2391.
- [43] R. A. Abate, T. Hung, P. Mary, J. J. Agresti, D. A. Weitz, *Proc. Natl. Acad. Sci. USA* **2011**, *107*, 19163–19166.
- [44] D. Peacock, D. Boulter, *Biochem. J.* **1970**, *120*, 763–769.
- [45] N. Kato, H. Sahm, F. Wagner, *Biochim. Biophys. Acta Enzymol.* **1979**, *566*, 12–20.
- [46] D. Zwicker, R. Seyboldt, C. A. Weber, A. A. Hyman, F. Jülicher, *Nat. Phys.* **2017**, *13*, 408–413.

Manuscript received: March 31, 2020

Version of record online: ■■■, ■■■■

ARTICLES



Dr. T. Beneyton, C. Love, Dr. M. Girault, Dr. T.-Y. D. Tang, Prof. J.-C. Baret**

1 – 9

High-Throughput Synthesis and Screening of Functional Coacervates Using Microfluidics



Open reaction centers: Droplet-based microfluidics allows the high-throughput synthesis and screening of populations of micron-sized coacervates with an unprecedented accuracy. The study of partition coefficients and se-

questered reaction rates in these minimal synthetic organelles provides insights in the role of sub-compartmentalisation in regulating out-of-equilibrium behaviours in biological systems.
